

Paper

Extended Joint Bilateral Filter for the Reduction of Color Bleeding in Compressed Image and Video

Naofumi Wada† (member), Masato Kazui† and Miki Haseyama†† (member)

Abstract In this paper, we propose a simple and effective technique, named extended joint bilateral filter, for reducing color bleeding which is defined as a smearing of the color between areas of strongly contrasting chroma in lossy-compressed images. The color bleeding comes from not only quantization but also sub-sampling in the YCbCr 4:2:0 color format. In order to deal with the two problems simultaneously, we extend the joint bilateral filter formulation by referring all of Y, Cb and Cr components based on a correlation between luma and chroma. As a result, our method achieves both noise reduction and sharpness enhancement for chroma without color edge blurring. Experimental results show that our method is effective in terms of both objective quality and subjective quality.

Keywords: image and video compression, bilateral filter, joint bilateral filter, color bleeding, denoising, post-processing.

1. Introduction

The resolution of imaging devices and display devices has been increasing over the years. 4K TVs and 8K Super Hi-Vision have emerged for applications of ultra-high definition video beyond Full-HD video. In this situation, a compression technique is a key technology to make a huge amount of data compact enough for the transmission bandwidth. International standards of codecs such as JPEG [1], JPEG2000 [2], MPEG-2 [3] and H.264/AVC [4] have widely used in the world, and H.265/HEVC [5] reported in 2013 has realized double the efficiency of H.264/AVC and has attracted attention as an advanced technique for providing 4K/8K videos. A common feature of the codecs is that transform coefficients are quantized to decrease the size of data after transforming an image to a frequency domain by DCT or Wavelet. In this process, the high frequency information to which human eyes are less sensitive is mainly quantized, and the amount of the data is effectively compressed while preserving the quality. Color information is also decreased efficiently for compression by using YCbCr color format which consists of luma (Y) and chroma (Cb, Cr) components. The chroma components are subsampled based on the human visual system that takes advantage of lower acuity for chroma differences than for luma [6]. Figure 1 shows an illustration of three color formats, 4:4:4, 4:2:2 and 4:2:0. In 4:4:4 (a), all components have the same resolution, but chroma components are subsampled in 4:2:2 (b) in a horizontal direction and in 4:2:0 (c) in horizontal and vertical directions. In the codecs, YCbCr 4:2:0 color format is generally used; the resolution of chroma images is a quarter of that of luma before encoding.

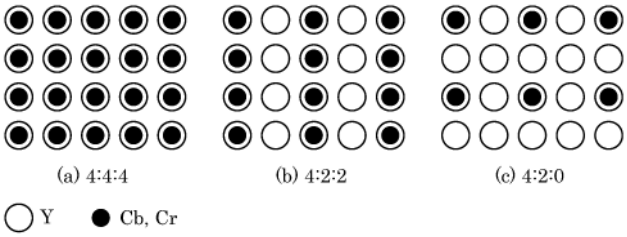

Fig. 1 Illustrations of YCbCr color formats.

Fig. 2 (a) Example of color bleeding and (b) Result of our approach.

Lossy compression, meanwhile, generates image degradation when compression rate is high. The existing

Received September 10, 2014; Revised November 6, 2014; Accepted December 4, 2014

† Samsung R&D Institute Japan Co. LTD. (Yokohama, Japan)
†† Hokkaido University (Sapporo, Japan)

works [7) 8)] made it clear that various types of compression artifacts. In particular, the degradation of color is called "color bleeding", which is usually defined as leakage of color across object boundaries, i.e., it appears as a smearing of the color between areas of strongly contrasting chroma. Figure 2 (a) shows an example of color bleeding. Color bleeding is caused by two problems of coding algorithm: quantization and subsampling of chroma. The first problem is that degradation of chroma image quality is conspicuous at a high compression rate. For this problem, many techniques to reduce noise by post-processing for decoded pictures have been proposed. For instance, non-linear filters such as a bilateral filter [9)] and an epsilon filter [10)] have been devised to smooth images while preserving edges. Kernel regression [11)] changes the kernel direction of a smoothing filter along with edge directions. A deblocking filter [12)] detects and reduces block noise. DCT denoising [13)] and SA-DCT denoising [14)] cut the coefficients of noise in the frequency domain. Non-local means [15)] and BM3D [16)] average small patches that have similar structures in the spatial and/or temporal domain. Optimization-based methods such as total variation minimization [17)] reduce artifacts by minimizing a cost function to solve the inverse problem. The second problem is that the chroma images are blurred due to the upscaling process when 4:2:0 is transformed to 4:4:4 on the display. Although interpolation filters, such as nearest neighbor, bi-linear and bi-cubic, are generally used for upscaling, they are insufficient for creating details and sharp edges due to the sampling theorem. Demosaicking, which reconstruct a full color image from a color filter array, is one of the interpolation techniques, and many approaches has been proposed for preventing false color and blur. Restoration-based methods model the degradation process and obtain a solution by solving inverse problem. Recently, numerous super-resolution techniques outperforming the conventional interpolation method have been presented. There are various super-resolution approaches such as frequency domain-based, compressed sensing, example-based and multi-frame [18) 19)].

However, most of the effective techniques for denoising and upscaling tend to have the drawback of high computational cost. It is inefficient to apply a high-complexity post-processor to not only luma component but also two chroma components. A simple and low-cost process is generally applied for chroma because it is difficult for the human eye to detect color difference, but color bleeding is perceived prominently around strong and vivid color edges in color text superimposed over the image, cel-animation and computer graphics. Hence, it is necessary to satisfy the following functions for reducing color bleeding efficiently: (i) Realizing both denoising and upsampling with detail enhancement simultaneously (ii) Saving computational cost (iii) Removing salient color artifacts around color edges.

In this paper, we propose a simple and effective filtering technique, named extended joint bilateral filter, which can effectively reduce color bleeding while saving computational cost without preprocessing such as edge detection. We show an example of our result in Fig. 2 (b). Our proposed method is an extension of the smoothing filter based on the framework of a joint bilateral filter [21)] with the addition of luma and chroma images as guides. Consequently, both noise reduction and sharpness enhancement for chroma images can be realized while suppressing side-effects such as blur. In addition, the proposed method, which is suitable for both software and hardware implementation, would be able to be applied for UHD video applications.

This paper is organized as follows. Section 2 introduce the existing bilateral filter, the data fusion approaches such as joint bilateral filter, and the existing color bleeding reduction related to our proposed method. In Section 3, we show the framework for improving color image quality using a joint bilateral filter. Then, we explain the algorithm and effects of our proposed extended joint bilateral filter. Experimental results for JPEG images are presented in Section 4. Finally, we conclude this paper in Section 5.

2. Related Works

2.1 Bilateral Filter

The bilateral filter [9)] which has been proposed by Tomasi et al. is a nonlinear filter to smooth images while preserving edges. The bilateral filter is closely related to a gaussian filter, which is a weighted averaging of pixels in local areas. When I denotes the input image and $f[I]$ denotes the output image of filter f applied to the image I, the gaussian filter is formulated as follows:

$$f[I]_{\mathbf{p}} = \frac{1}{W_p} \sum_{\mathbf{q} \in \Omega} G_\sigma \left(\left\| \mathbf{p} - \mathbf{q} \right\| \right) \cdot I_{\mathbf{q}} \ , \qquad (1)$$

where $\mathbf{p}$ is the pixel position at the center of the filter kernel and $\mathbf{q}$ is the pixel position in the region Ω. I_q is the image value at pixel position $\mathbf{q}$. $\| x \|$ means the L_2 norm of x, e.g., $\| \mathbf{p} - \mathbf{q} \|$ is the Euclidean distance between pixel locations $\mathbf{p}$ and $\mathbf{q}$. Normalization factor W_p ensures pixel weights sum to 1.0. G_σ is a 2D gaussian

kernel given by

$$G_\sigma(x) = \frac{1}{\sqrt{2\pi\sigma^2}} \exp\left(-\frac{x^2}{2\sigma^2}\right), \quad (2)$$

where the parameter σ denotes standard deviation of the gaussian distribution. The gaussian filter is the simplest low-pass filter used for removing noise in images. The further the distance is from the center pixel **p**, the smaller is the weight applied for the pixels in the area Ω. The strength of this influence depends only on the spatial distance between **p** and **q**. As a result, image edges are blurred because pixels across discontinuities are averaged together.

On the other hand, the bilateral filter is formulated as follows:

$$f[I]_{\mathbf{p}} = \frac{1}{W_{\mathbf{p}}} \sum_{\mathbf{q}\in\Omega} G_{\sigma_s}\left(\|\mathbf{p}-\mathbf{q}\|\right) \cdot G_{\sigma_r}\left(\left|I_{\mathbf{p}} - I_{\mathbf{q}}\right|\right) \cdot I_{\mathbf{q}}, \quad (3)$$

where I_p is the image value at **p** and $|x|$ is the absolute value of x. Normalization factor W_p ensures pixel weights sum to 1.0. As shown in the above equations, the bilateral filter consists of two weights, geometric weight, $G_{\sigma s}$, in the spatial domain and photometric weight, $G_{\sigma r}$, in the range domain; the smoothing effect becomes weak when the difference of intensity value is large between **p** and **q**. Hence, the bilateral filter can perform smoothing while preserving edges. The bilateral filter is a very simple method depending only on two parameters, σ_s and σ_r, without an iterative manner. Therefore, the bilateral filter is tractable and highly extensible, so that it has been used for various applications such as tone management, texture editing, demosaicking and stylization as well as denoising. Furthermore, a great number of fast algorithms have also been proposed [20].

2.2 Data Fusion

A joint bilateral filter [21] has been proposed by Petschnigg et al. as an extension of the bilateral filter (Eisemann et al. [22] have proposed a similar technique, named cross bilateral filter). The joint bilateral filter is different from the bilateral filter in that a guidance image is used instead of a filtered image for calculating photometric weights. In their work, flash and no-flash images are used for reducing noise in low-light conditions in digital photography. Given a flash image F and a no-flash image I, the equation of the joint bilateral filter is formulated as follows:

$$f[I]_{\mathbf{p}} = \frac{1}{W_{\mathbf{p}}} \sum_{\mathbf{q}\in\Omega} G_{\sigma_s}\left(\|\mathbf{p}-\mathbf{q}\|\right) \cdot G_{\sigma_r}\left(\left|F_{\mathbf{p}} - F_{\mathbf{q}}\right|\right) \cdot I_{\mathbf{q}}. \quad (4)$$

The key idea is to extract clear details of the flash image and combine them with natural-looking color of the noisy no-flash image while reducing noise.

Kopf et al. [23] have proposed a joint bilateral upsampling, which uses a full resolution guidance image for upscaling a downsampled input image, as an extension of the joint bilateral filter. This technique can produce a better full resolution results and can save computation time without pre-upscaling before filtering.

Bennett et al. [24] have proposed a dual bilateral filter which uses an infra-red image in addition to a visible image in order to denoise images in low-light conditions. The dual bilateral filter is formulated as follows:

$$f[I]_{\mathbf{p}} = \frac{1}{W_{\mathbf{p}}} \sum_{\mathbf{q}\in\Omega} G_{\sigma_s}\left(\|\mathbf{p}-\mathbf{q}\|\right) \cdot G_{\sigma_{rI}}\left(\left|Y_{\mathbf{p}} - Y_{\mathbf{q}}\right|\right) \cdot G_{\sigma_{rIR}}\left(\left|IR_{\mathbf{p}} - IR_{\mathbf{q}}\right|\right) \cdot I_{\mathbf{q}}, \quad (5)$$

where Y is a value of the luma image in YCbCr color space and IR is an intensity of the infra-red image. The dual bilateral filter reduces noise and enhances details in the noisy visible image by utilizing the infra-red image including sharp edges in low-light conditions.

He et al. [25] have proposed a guided filter which has similar effects to the above data fusion techniques. This technique has a fast and non-approximate linear-time algorithm. By using integral image, its computational cost is low and is independent from its kernel size.

The framework of data fusion, which use the guidance image differing from the input image, has been used in various applications such as detail enhancement, HDR compression, image matting, feathering, haze removal, demosaicking and colorization [20) 25)].

2.3 Color Bleeding Reduction

In this section, we introduce existing researches related to the color bleeding reduction. Coudoux et al. have proposed a block-based filtering method in DCT-domain, which may be subject to color bleeding by classifying block patterns [30) 31) 32)]. Spampinato et al. have proposed a pixel-based filtering method based on a fuzzy filter employing the edge information detected by the sobel filter and the chroma distance to determine the weights of filter kernel [33) 34)]. Li et al. have similarly proposed a filtering method weighted by the luma edges and chroma distance [35)]. These methods are based on an assumption that strong chroma edges are accompanied by strong luma edges for natural images, as well as our approach.

However, the above methods need to localize the color bleeding areas beforehand by pre-processing such as edge detection. In addition, we need to not only reduce

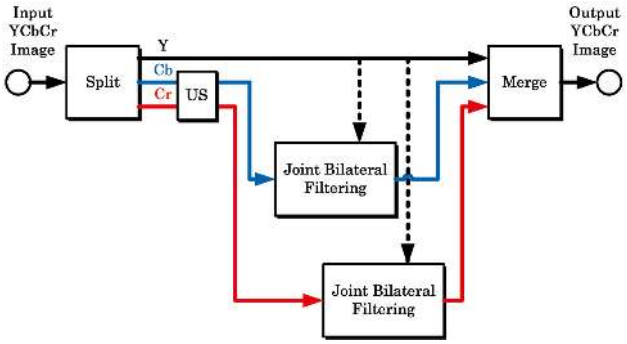

Fig. 3 Block diagram of the filtering process for chroma images based on joint bilateral filtering.

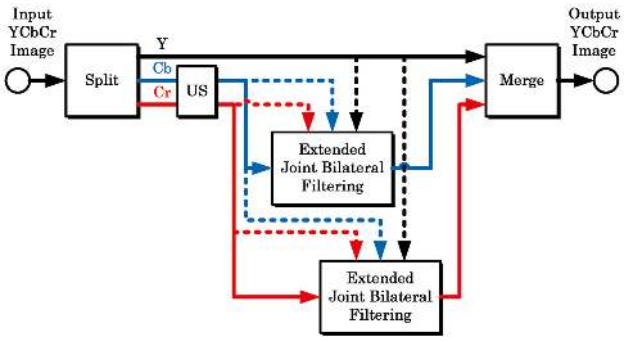

Fig. 4 Block diagram of the filtering process for chroma images based on extended joint bilateral filtering.

noise but also restore the sharpness of color edges in order to improve the blurriness of the sub-sampled chroma image particularly in the images containing high-contrast color edges. For these problems, we adopt the data fusion framework described in the preceding subsection. Next section gives the detail explanation of our approach.

3. Proposed Method

3.1 Joint Bilateral Filter for Color Debleeding

As we have stated in Section 1, compressed chroma images include color bleedings due to quantization and sub-sampling. Therefore, restoration of details while reducing artifacts is needed for chroma images. However, it is inefficient to apply the existing high-complexity denoising and super-resolution algorithm to all Y, Cb and Cr components in terms of computational cost. For these problems, we propose a computationally low-cost and simple algorithm to improve the quality of chroma images by utilizing the framework of the joint bilateral filter (JBF) described in Subsection 2.2. Specifically, we apply a smoothing filter for chroma while using luma as a guide based on a high correlation between luma and chroma edges. Given a luma image Y and a filtering target chroma image C (Cb or Cr), a JBF for color debleeding can be formulated as follows:

$$f[C]_{\mathbf{p}} = \frac{1}{W_{\mathbf{p}}} \sum_{\mathbf{q}\in\Omega} G_{\sigma_s}\left(\|\mathbf{p}-\mathbf{q}\|\right) \cdot G_{\sigma_r}\left(\left|Y_{\mathbf{p}} - Y_{\mathbf{q}}\right|\right) \cdot C_{\mathbf{q}} \,. \quad (6)$$

Figure 3 shows a block diagram of the filtering process for chroma images by the JBF. The process US in Fig. 3 denotes upscaling with the conventional interpolation method (e.g. bilinear filtering) which provides C in (6) with the same resolution as Y. The black dotted lines in Fig. 3 denote that the JBF uses the luma image Y as a guide. By taking into account clear details and sharp edges of luma, the JBF performs noise reduction and detail enhancement simultaneously for chroma images.

Such a technique which improves the image quality of low-resolution channel by referring high-resolution channel is also utilized for demosaicking and colorization. Demosaicking reconstructs a full color image from the incomplete color samples of color filter array. Kiku et al. [26] have used a guided filter [25] to interpolate R and B images by referring G image as a guidance image. The purpose of demosaicking is to interpolate the missing pixels, and it is required to preserve original image structure while suppressing false color with robustness for noise at high-sensitivity photography. Colorization adds color to a monochrome image. This technique interpolates extremely sparse chroma pixels by referring a full-resolution luma image. For instance, joint bilateral upsampling [23] and guided filter [25] have been proposed. Although the concept of demosaicking and colorization is similar to ours, the aim of our research is not only interpolation but also color bleeding reduction, i.e., both denoising and upsampling with detail reconstruction. We introduce color debleeding as a new application of the data fusion framework such as joint bilateral filter. However, we found that the original joint bilateral filter in (6) generates a serious problem as a side-effect. We describe this problem in detail and propose an extension for solving it in the following subsection.

3.2 Extended Joint Bilateral Filter

First, we consider the definition of denoising probabilistically in order to clear the problem of the JBF in (6) stated in the preceding subsection. In terms of denoising, it is generally required that both a target pixel and reference pixels to be smoothed should be in a uniform region. In other words, the property of the filter is decided how "uniformity" is defined. For instance, the gaussian filter in (1) defines the uniformity based only on a spatial distance, and a gaussian distribution is used as a dissimilarity measure. Also, the bilateral filter in

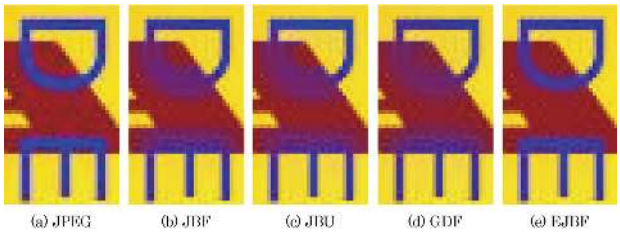

Fig. 5 Comparison of filtering results in luma flat area with color edges: (a) JPEG compressed image, (b) joint bilateral filter, (c) joint bilateral upsampling, (d) guided filter, and (e) extended joint bilateral filter.

(3) defines the uniformity based on not only spatial distance but also similarity of pixel value. Here, we consider the definition of (6) probabilistically. The event $U_{\mathbf{p},\mathbf{q}}$ denotes that both samples **p** and **q** lie in the same uniform region. Suppose the weight of (6) can be represented by the conditional probability $\mathrm{P}(U_{\mathbf{p},\mathbf{q}}|Y)$, it can be expressed in the following formula by using Bayes' theorem:

$$\mathrm{P}(U_{\mathbf{p},\mathbf{q}}|Y) \propto \mathrm{P}(U_{\mathbf{p},\mathbf{q}}) \cdot \mathrm{P}(Y|U_{\mathbf{p},\mathbf{q}}). \quad (7)$$

Here, we assume that both the probability distribution of $\mathrm{P}(U_{\mathbf{p},\mathbf{q}})$ and the likelihood function of $\mathrm{P}(Y|U_{\mathbf{p},\mathbf{q}})$ are gaussian distributions as well as bilateral filter, i.e., $\mathrm{P}(U_{\mathbf{p},\mathbf{q}}) = \mathrm{G}_{\sigma_s}(\|\mathbf{p}-\mathbf{q}\|)$ and $\mathrm{P}(Y|U_{\mathbf{p},\mathbf{q}}) = \mathrm{G}_{\sigma_r}(|Y_\mathbf{p}-Y_\mathbf{q}|)$ are obtained by (6) and (7) respectively. Evidently, when $\mathrm{P}(Y|U_{\mathbf{p},\mathbf{q}})$ is large: the similarity of luma values between p and q is high, $\mathrm{P}(U_{\mathbf{p},\mathbf{q}}|Y)$ depends mainly on $\mathrm{P}(U_{\mathbf{p},\mathbf{q}})$. In other words, the JBF in (6) becomes a gaussian filter when $Y_\mathbf{p}$ and $Y_\mathbf{q}$ are the same value. As a result, it would be a serious problem that color edges are blurred in luma flat region. Note that both joint bilateral upsampling [23] and guided filter [25] also have the same problem. Figure 5 shows the experimental results in luma flat region including chroma edges. In Fig. 5, the methods (b), (c) and (d) generate terrible blur of color edge as a side-effect in the area where the red and blue characters overlapped.

In order to solve this problem, we extend (6) for taking into account the similarities of all components. The probability $\mathrm{P}(U_{\mathbf{p},\mathbf{q}}|Y, Cb, Cr)$, which is the uniformity of the samples **p** and **q**, is represented as the following formula based on Bayes' theorem as well as (7):

$$\mathrm{P}(U_{\mathbf{p},\mathbf{q}}|Y,Cb,Cr) \propto \mathrm{P}(U_{\mathbf{p},\mathbf{q}}) \cdot \mathrm{P}(Y,Cb,Cr|U_{\mathbf{p},\mathbf{q}}), \quad (8)$$

Here, the values of Y, Cb and Cr are independent; the noises included in each component are also independent because Y, Cb and Cr are encoded individually. Assuming the conditional independence, (8) is rewritten as

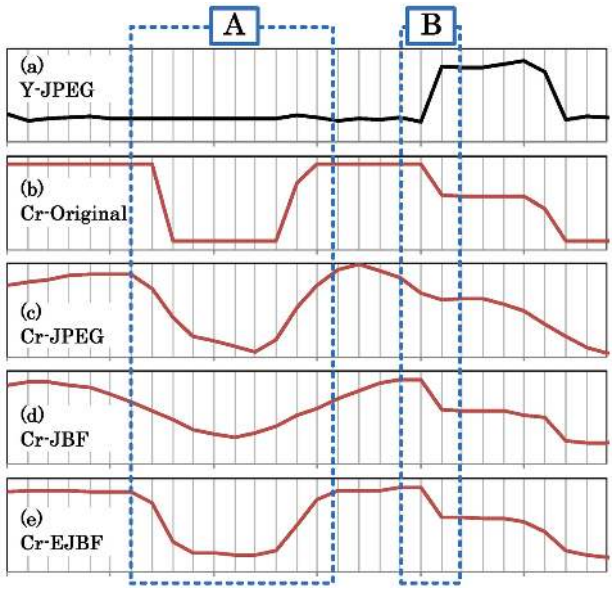

Fig. 6 1-D illustration for pixel values of (a) Y coded by JPEG, (b) Uncompressed Cr, (c) Cr coded by JPEG, (d) Cr filtered by JBF and (e) Cr filtered by EJBF. See the text for detailed explanation.

$$\mathrm{P}(U_{\mathbf{p},\mathbf{q}}|Y,Cb,Cr) \propto \mathrm{P}(U_{\mathbf{p},\mathbf{q}}) \cdot \mathrm{P}(Y|U_{\mathbf{p},\mathbf{q}}) \cdot \mathrm{P}(Cb|U_{\mathbf{p},\mathbf{q}}) \cdot \mathrm{P}(Cr|U_{\mathbf{p},\mathbf{q}}). \quad (9)$$

The likelihood functions of $\mathrm{P}(Cb|U_{\mathbf{p},\mathbf{q}})$ and $\mathrm{P}(Cr|U_{\mathbf{p},\mathbf{q}})$ are gaussian distribution as well as $\mathrm{P}(Y|U_{\mathbf{p},\mathbf{q}})$. From (9), it is clear that $\mathrm{P}(U_{\mathbf{p},\mathbf{q}}|Y, Cb, Cr)$ will be small if at least one of $\mathrm{P}(Y|U_{\mathbf{p},\mathbf{q}})$, $\mathrm{P}(Cb|U_{\mathbf{p},\mathbf{q}})$ and $\mathrm{P}(Cr|U_{\mathbf{p},\mathbf{q}})$ is small due to edges. On the basis of the above definition, we propose a new filtering technique named extended joint bilateral filter (EJBF) [36], which is defined as follows:

$$f[C]_\mathbf{p} = \frac{1}{W_\mathbf{p}} \sum_{\mathbf{q}\in\Omega} G_{\sigma_s}(\|\mathbf{p}-\mathbf{q}\|) \cdot G_{\sigma_{r0}}(|Y_\mathbf{p}-Y_\mathbf{q}|) \cdot G_{\sigma_{r1}}(|Cb_\mathbf{p}-Cb_\mathbf{q}|) \cdot G_{\sigma_{r2}}(|Cr_\mathbf{p}-Cr_\mathbf{q}|) \cdot C_\mathbf{q}. \quad (10)$$

where σ_{r0}, σ_{r1} and σ_{r2} are standard deviations for photometric weights of Y, Cb and Cr, respectively. Figure 4 shows a block diagram of our EJBF for chroma images. Our EJBF is different from the JBF with regard to guide image, i.e., our EJBF uses both of luma and chroma components as guide images while the JBF uses only luma. The black, blue and red dotted lines in Fig. 4 denote that our EJBF uses Y, Cb and Cr as guides, respectively. Consequently, as shown in Fig. 5 (e), our EJBF can provide both of smoothing and edge preserving effect in luma flat area.

We explain the effects of our EJBF in detail by using Fig. 6. The graphs of Fig. 6 show 1-D profiles of pixel values; the horizontal axis denotes pixel position and the vertical axis denotes intensity. The graph (a) shows the pixel values of luma Y for JPEG image and (b)-(e) show

Fig. 7 Test images for our experiment.

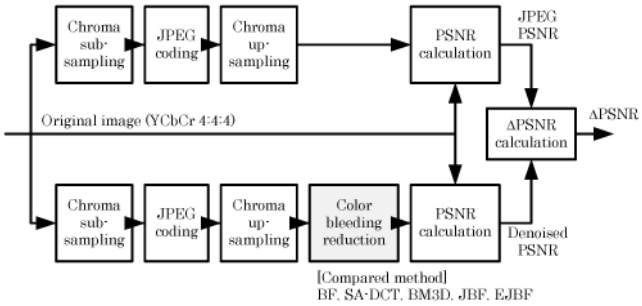

Fig. 8 Block diagram for calculating ΔPSNR.

Table 1 Parameters for our experiment.

Method	Parameter
BF [9]	σ_s=4, σ_r=0.03
SA-DCT [14]	Block=8x8, σ=7
BM3D [16]	Block=8x8, σ=7
JBF	σ_s=4, σ_r=0.03
EJBF	σ_s=4, σ_r=0.03, σ_{r1}=σ_{r2}=0.10

that of Cr. The graph (b) shows the uncompressed original image of 4:4:4 color format. The graph (c) shows Cr profile of JPEG, and (d) and (e) show Cr profiles filtered by the JBF and our EJBF respectively. In the case of (c), (d) and (e), the chroma components are upscaled. We focus on region A and B enclosed by dotted boxes in Fig. 6. In region A, the JBF blurs Cr edge as shown in (d) due to limitation of the JBF described above. On the other hand, our EJBF can preserve edge as shown in (e). In region B, blurriness is occurred in (c) due to sub-sampling of JPEG compression. Both the JBF and our EJBF can successfully reproduce the sharp edge of chroma corresponding to uncompressed original edge because of an existing sharp edge in luma.

As described above, our EJBF can achieve denoising and sharpness enhancement simultaneously for chroma components without side-effect such as edge blur. Other merits of our EJBF are simplicity and usability. Because the algorithm of our EJBF is based on bilateral filter, acceleration methods would be able to be utilized for implementation. For instance, a separable filtering [37] can be applied due to the simple multiplication of gaussian functions in (10). Also, upscaling process, US in Fig. 4, can be omitted by using the joint bilateral upsampling [23] instead of joint bilateral filter, i.e., chroma pixels before upscaling are used in (10). A parallel processing method of bilateral filtering on multi-core CPUs or GPUs [38] would also be able to be used for acceleration of our EJBF. According to the above acceleration methods, our proposed method is effective and suitable for real-time UHD video applications.

4. Performance Evaluation

4.1 Experimental Conditions

In this section, we show the performance of our proposed method for color bleeding reduction using still images compressed by JPEG. We used seven uncompressed YCbCr 4:4:4 images shown in Fig. 7 as original images for our experiment. They contain four natural images (Caps, Bike, Rafting and Parrots) and three artificial images (Beehive, Color text, Color bars). The natural images were selected from Kodak Lossless True Color Image Suite [39] which contains 24 images with 768×512 pixels considering its wide variety of colors. The artificial images were made assuming color text superimposed over the image or cel-animation. The size of each image was 256×256 pixels. In particular, the artificial image "Beehive" has been designed by Punchihewa et al. as a test pattern image to evaluate color bleeding artifact [27) 28) 29)]. This consists of hexagons arranged in a beehive pattern. The colors of hexagons are red, green, blue, cyan, magenta, yellow and white. This image shows the color bleeding artifact around many color boundaries after coding. We compressed the original images by using version 9 of JPEG reference software [40] provided by the Independent JPEG Group (IJG). Parameters of the software were set as follows: chroma sub-sampling was 4:2:0 and quality control parameter N was changed; the default value of N was 75 in the software. The smaller N becomes, the higher

Table 2 Results of ΔPSNR (N=75).

Image	Cb-ΔPSNR					Cr-ΔPSNR					Average ΔPSNR				
	BF	SA-DCT	BM3D	JBF	EJBF	BF	SA-DCT	BM3D	JBF	EJBF	BF	SA-DCT	BM3D	JBF	EJBF
N1	0.43	0.85	0.85	0.56	**1.01**	0.16	**0.88**	0.86	-0.57	0.36	0.29	**0.87**	0.85	-0.01	0.68
N2	-0.17	0.18	**0.43**	-0.37	-0.01	-0.01	0.32	**0.58**	-0.75	-0.18	-0.09	0.25	**0.51**	-0.56	-0.09
N3	0.09	0.45	**0.57**	-0.53	0.28	-0.08	0.41	**0.48**	-1.97	-0.46	0.01	0.43	**0.53**	-1.25	-0.09
N4	0.16	**0.64**	0.57	-0.19	0.62	0.00	**0.70**	0.67	-0.48	0.24	0.08	**0.67**	0.62	-0.34	0.43
A1	0.57	0.75	0.31	**2.66**	2.39	0.65	0.93	0.33	**3.42**	2.60	0.61	0.84	0.32	**3.04**	2.50
A2	0.22	0.24	0.08	**1.56**	1.41	0.32	0.36	0.31	-0.57	**1.87**	0.27	0.30	0.19	0.50	**1.64**
A3	0.69	0.49	0.21	2.24	**4.08**	0.61	0.51	0.17	3.18	**5.00**	0.65	0.50	0.19	2.71	**4.54**
Ave. N	0.13	0.53	**0.60**	-0.13	0.48	0.02	0.58	**0.65**	-0.94	-0.01	0.07	0.56	**0.63**	-0.54	0.23
Ave. A	0.49	0.49	0.20	2.15	**2.63**	0.53	0.60	0.27	2.01	**3.16**	0.51	0.54	0.23	2.08	**2.89**
Ave. All	0.28	0.52	0.43	0.85	**1.40**	0.24	0.59	0.49	0.32	**1.35**	0.26	0.55	0.46	0.58	**1.37**

Table 3 Results of ΔPSNR (N=50).

Image	Cb-ΔPSNR					Cr-ΔPSNR					Average ΔPSNR				
	BF	SA-DCT	BM3D	JBF	EJBF	BF	SA-DCT	BM3D	JBF	EJBF	BF	SA-DCT	BM3D	JBF	EJBF
N1	0.56	0.92	0.75	1.06	**1.33**	0.52	0.68	0.55	0.21	**0.89**	0.54	0.80	0.65	0.63	**1.11**
N2	0.22	0.46	**0.53**	0.26	0.49	0.26	0.57	**0.64**	-0.03	0.32	0.24	0.52	**0.59**	0.11	0.40
N3	0.24	0.45	0.47	0.29	**0.76**	0.07	0.43	**0.43**	-0.78	0.18	0.16	0.44	0.45	-0.24	**0.47**
N4	0.48	0.77	0.62	0.55	**1.02**	0.33	**0.79**	0.67	0.20	0.69	0.41	0.78	0.65	0.37	**0.85**
A1	0.46	0.51	0.31	**2.57**	1.99	0.55	0.63	0.34	**3.22**	2.19	0.51	0.57	0.32	**2.90**	2.09
A2	0.22	0.21	0.10	**1.55**	1.26	0.06	0.19	0.22	0.30	**1.53**	0.14	0.20	0.16	0.93	**1.39**
A3	0.72	0.41	0.22	2.30	**3.51**	0.72	0.44	0.19	3.07	**4.30**	0.72	0.43	0.20	2.68	**3.91**
Ave. N	0.38	0.65	0.59	0.54	**0.90**	0.30	**0.62**	0.58	-0.10	0.52	0.34	0.63	0.58	0.22	**0.71**
Ave. A	0.46	0.38	0.21	2.14	**2.25**	0.44	0.42	0.25	2.20	**2.68**	0.45	0.40	0.23	2.17	**2.46**
Ave. All	0.41	0.53	0.43	1.23	**1.48**	0.36	0.53	0.44	0.88	**1.44**	0.39	0.53	0.43	1.05	**1.46**

Table 4 Results of ΔPSNR (N=25).

Image	Cb-ΔPSNR					Cr-ΔPSNR					Average ΔPSNR				
	BF	SA-DCT	BM3D	JBF	EJBF	BF	SA-DCT	BM3D	JBF	EJBF	BF	SA-DCT	BM3D	JBF	EJBF
N1	0.55	0.92	0.70	1.17	**1.27**	0.51	0.62	0.42	0.52	**0.88**	0.53	0.77	0.56	0.84	**1.08**
N2	0.48	0.56	0.50	0.65	**0.75**	0.41	0.65	0.57	0.50	**0.67**	0.45	0.60	0.54	0.57	**0.71**
N3	0.43	0.49	0.44	0.77	**0.97**	0.12	0.31	0.28	-0.08	**0.40**	0.27	0.40	0.36	0.35	**0.69**
N4	0.74	0.76	0.54	0.85	**1.18**	0.49	0.80	0.61	0.63	**0.90**	0.62	0.78	0.57	0.74	**1.04**
A1	0.29	0.33	0.22	**2.21**	1.45	0.35	0.38	0.25	**2.79**	1.61	0.32	0.35	0.23	**2.50**	1.53
A2	0.14	0.14	0.08	**1.66**	1.01	0.07	0.17	0.18	0.69	**1.11**	0.11	0.15	0.13	**1.17**	1.06
A3	0.48	0.22	0.16	**2.62**	2.45	0.55	0.16	0.12	**3.37**	2.85	0.51	0.19	0.14	**2.99**	2.65
Ave. N	0.55	0.68	0.55	0.86	**1.04**	0.38	0.59	0.47	0.39	**0.71**	0.47	0.64	0.51	0.63	**0.88**
Ave. A	0.30	0.23	0.15	**2.16**	1.64	0.32	0.24	0.18	**2.28**	1.86	0.31	0.23	0.17	**2.22**	1.75
Ave. All	0.44	0.49	0.38	**1.42**	1.30	0.36	0.44	0.35	**1.20**	**1.20**	0.40	0.46	0.36	**1.31**	1.25

compression rate becomes. We compared the color bleeding reduction performance of the bilateral filter (BF) [9], the joint bilateral filter (JBF), and the proposed extended joint bilateral filter (EJBF). In addition, we compared SA-DCT [14] that is a frequency-based approach and BM3D [16] that is a patch-based approach as the state-of-the-art noise reduction methods. For an objective image quality index, we used Peak Signal-to-Noise Ratio (PSNR), which is generally used for image quality assessment in the field of noise reduction or image correction. PSNR was calculated based on the square error of the 4:4:4 uncompressed Cb/Cr image and the upscaled compressed Cb/Cr image. And also, we showed ΔPSNR, which is the difference of PSNRs of JPEG-coded image and of filtered image: ΔPSNR means an improvement degree from JPEG image quality. If the value is negative, it means image quality is worse than the JPEG image due to side-effects such as edge blurring

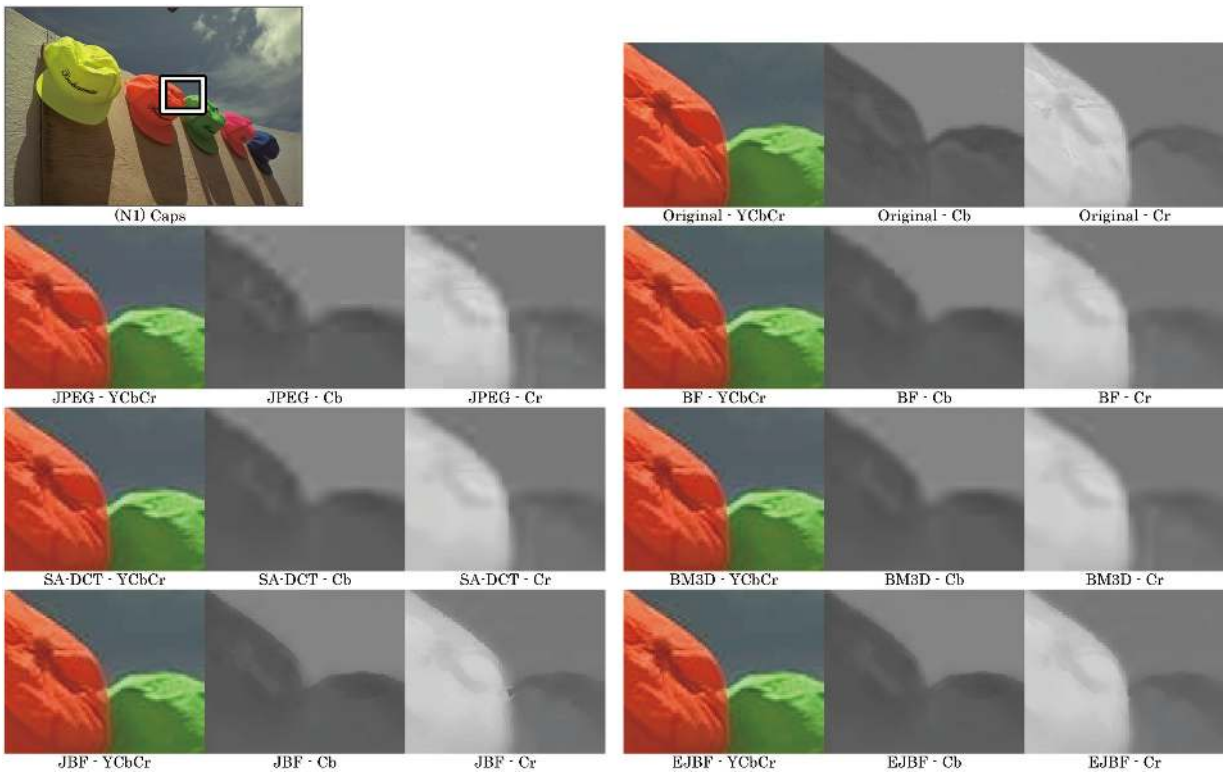

Fig. 9 Result images of natural image "Caps". YCbCr is color image. Cb and Cr are expressed by gray-scale.

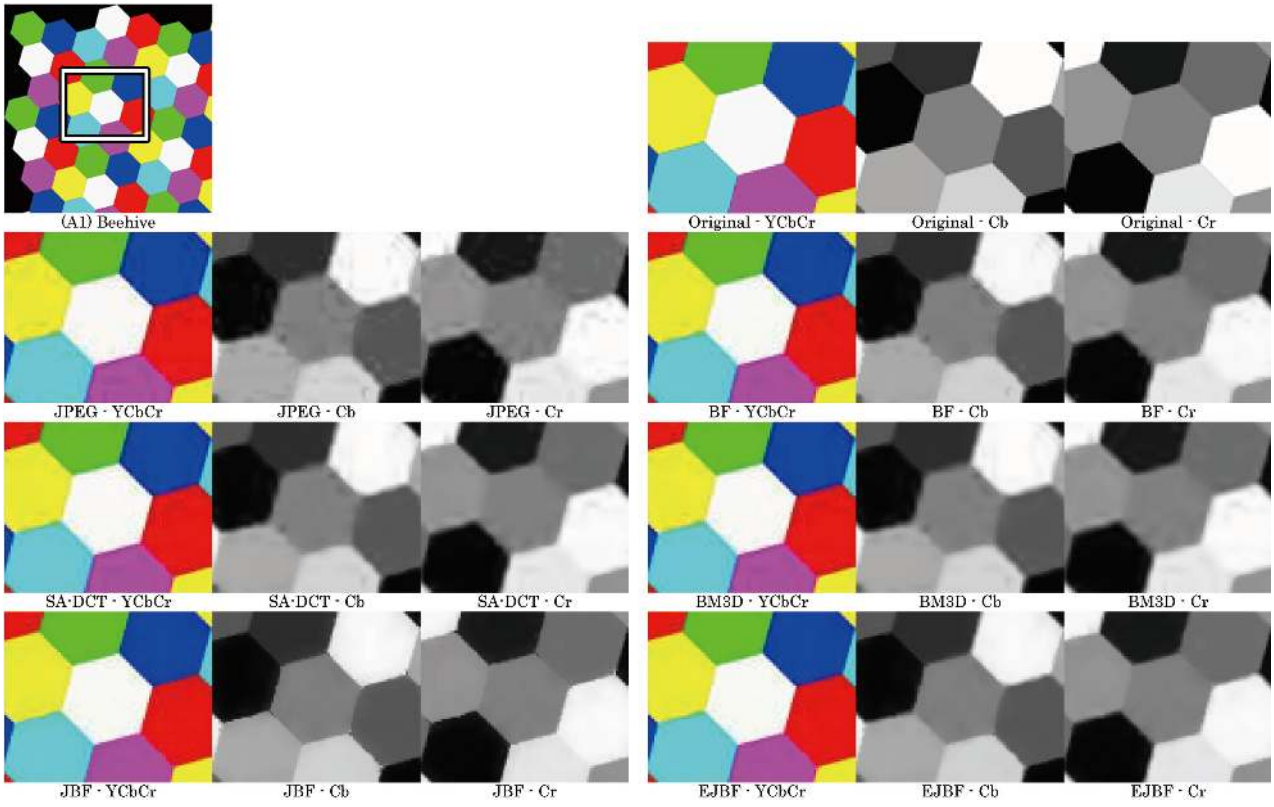

Fig. 10 Result images of artificial image "Beehive". YCbCr is color image. Cb and Cr are expressed by gray-scale.

or texture-loss. Figure 8 shows a block diagram for deriving ΔPSNR.

4.2 Experimental Results

First, we describe the objective quality evaluation. Table 1 shows the parameters of each method used in our experiment. We set these values empirically and used fixed parameters in following experiments. We measured ΔPSNR following the block diagram indicated in Fig. 8. Tables 2, 3 and 4 show the results of ΔPSNR for N=75, 50 and 25 respectively. It means that a

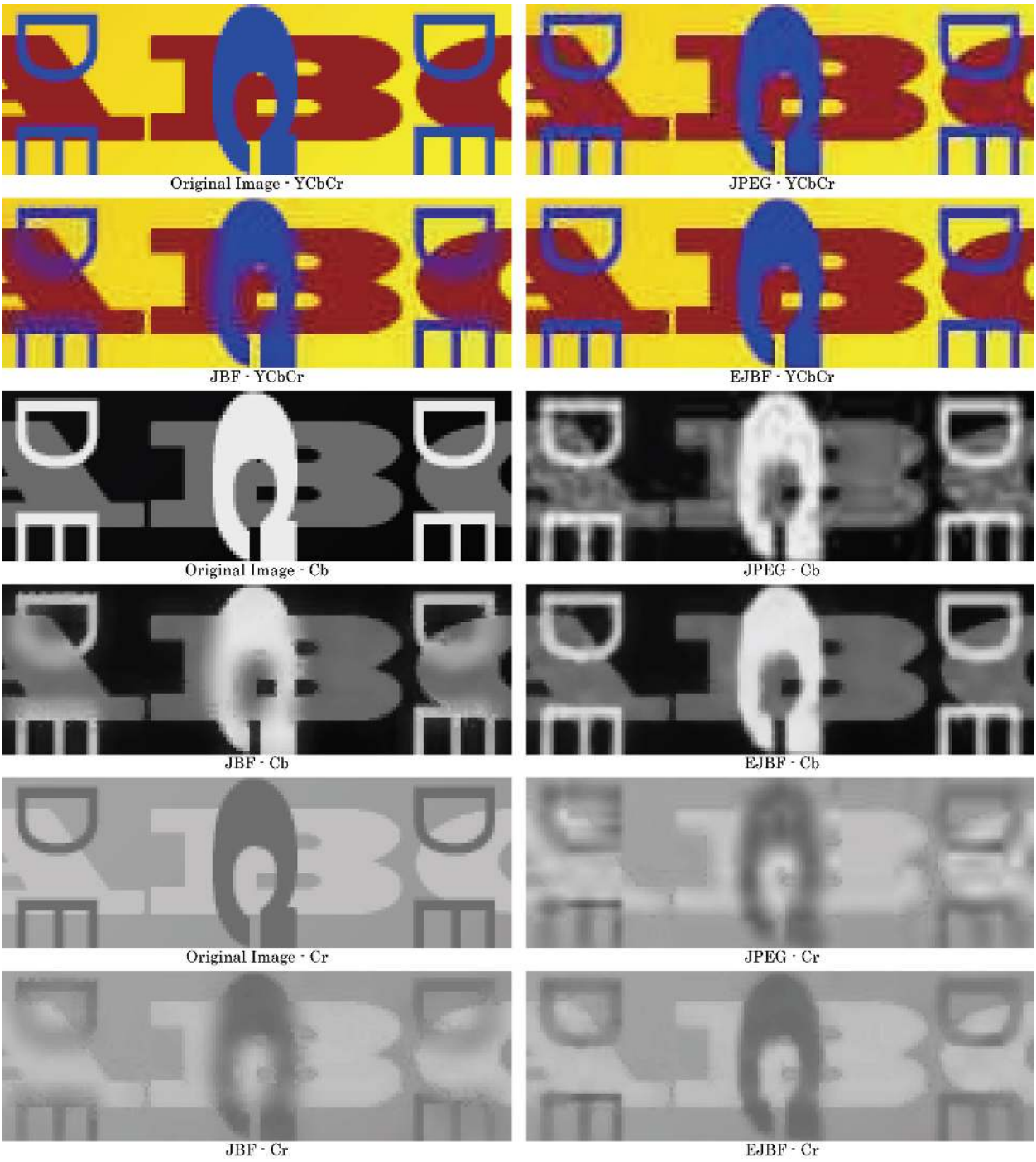

Fig. 11 Result images of artificial image "Color text". YCbCr is color image. Cb and Cr are expressed by gray-scale.

compression rate was changed by the quality control parameter N. In Table 2 (N=75), the SA-DCT and the BM3D show relatively higher ΔPSNR than other methods for natural images. The ΔPSNR of our EJBF was negative in N2 and N3 including many textures. We consider that our EJBF generates detail-loss at low compression rate, where original detailed textures in natural images relatively remain after compression, because the parameter of our EJBF in Table 1 has strong smoothing effect. The details for parameters of our EJBF will be discussed later. In contrast, ΔPSNRs of the JBF and our EJBF are extremely higher than other methods for the artificial images. This result shows that luminance information is effective for improving chroma image quality without side-effect in the artificial images which are consisted of flat region and sharp edges. On the other hand, in Tables 3 (N=50) and 4 (N=25), ΔPSNR of our EJBF tends to be higher than other methods for the natural images at high compression rates. As the compression rate becomes higher, dominant image structures remain after compression, whereas detailed textures are lost due to quantization. For this, texture-

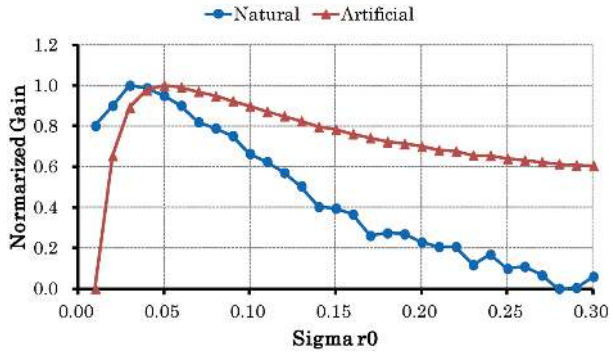

Fig. 12 Graph of normalized ΔPSNR vs. parameter sigma r0.

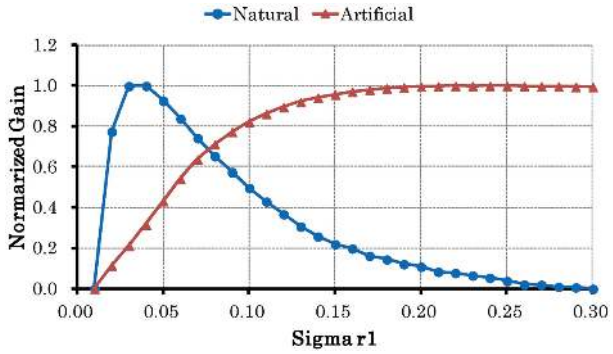

Fig. 13 Graph of normalized ΔPSNR vs. parameter sigma r1.

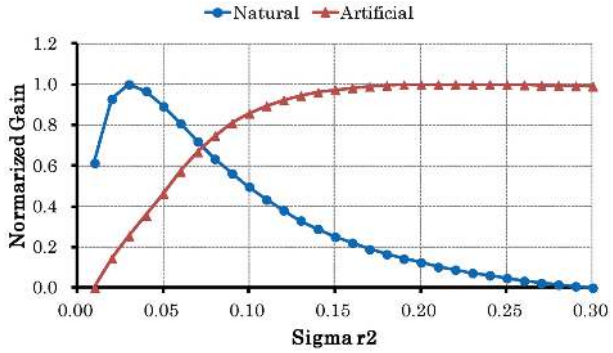

Fig. 14 Graph of normalized ΔPSNR vs. parameter sigma r2.

loss, the side-effect of smoothing, can be mostly ignored, and our EJBF can increase ΔPSNR in natural images as well as artificial images. While the average ΔPSNR of our EJBF for the natural images was under 1dB, it was over 1dB for artificial images in our experiments. These results show that the proposed method is effective particularly for images that contain various vivid colors and sharp color edges in comparison with the SA-DCT and the BM3D.

Next, we verified the effects for subjective quality. Figures 9 and 10 show the results using the natural image "Caps" and the artificial image "Beehive" with the parameter N=50. We focused on the white box areas of the upper left images in Figs. 9 and 10, and results of Cb

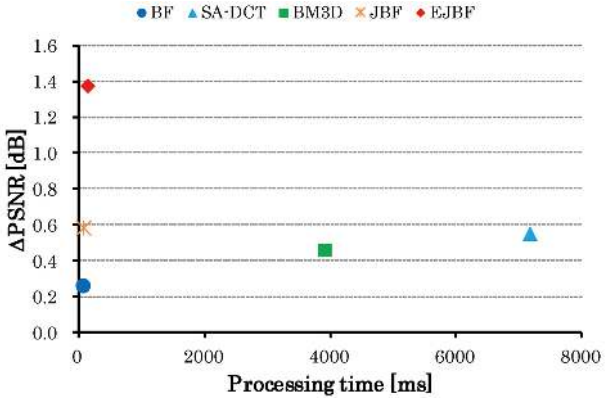

Fig. 15 Graph of ΔPSNR vs. processing time for each method.

Table 5 Comparison of processing time.
(CPU: Intel Xeon 3.50 GHz, Memory: 16GB)

Method	Processing time [ms]
BF [9]	69.6
SA-DCT [14]	7179.3
BM3D [16]	3913.4
JBF	69.0
EJBF	143.2

and Cr components are shown by gray-scale. In the JPEG compressed images, we can see image quality impairment such as color noise in chroma image, particularly around edges. Also sharpness and details are degraded due to upscaling for subsampled chroma images. Although the BF, the SA-DCT and the BM3D can reduce color noise around edges, it does not restore edge sharpness so that color bleeding is remaining. On the other hand, the JBF and our EJBF can restore edge sharpness while reducing color noise. Figure 11 shows the result of the artificial image "Color text". The JBF generates terrible blur of color edge in the area overlapping the red and blue characters due to no-edge in luma. As described in Subsection 3.2, it is cause of this problem that the JBF depends only on luma image to decide uniformity (joint bilateral upsampling and guided filter have the same problem). On the other hand, our EJBF can reduce color bleeding while suppressing the side-effect of blurriness.

Then, we verified the effect of the parameters σ_{r0}, σ_{r1} and σ_{r2} in (10) of our EJBF. In (10), σ_{r0}, σ_{r1} and σ_{r2} are the parameters for controlling photometric weights for Y, Cb and Cr respectively. Here, we measured ΔPSNR while changing one of these parameters under the condition that the other two parameters were fixed. Figures 12, 13 and 14 show the results for σ_{r0}, σ_{r1} and σ_{r2} respectively. The horizontal axis of graphs denotes σ and the vertical axis denotes ΔPSNR which is

normalized to the range of 0 to 1 within the range of σ in the graphs. The blue line shows the average ΔPSNR of the natural images N1~N4. The red line shows the average ΔPSNR of the artificial images A1~A3. In Fig. 12, ΔPSNR reached its peak at 0.03 of σ_{r0} and gradually decreased after 0.03 of σ_{r0} for the natural scene images. For the artificial images, ΔPSNR was at its peak around 0.05 of σ_{r0} and slowly decreased after 0.05 of σ_{r0}. Figures 13 and 14 show the same tendencies. The peak of ΔPSNR was around 0.03 of σ, and ΔPSNR was dramatically decreased after 0.03 of σ for the natural scene images. For the artificial images, however, ΔPSNR keeps increasing until 0.20 of σ and became stable after 0.20 of σ. The characteristics of σ in range domain are described in many previous researches regarding the bilateral filter [9) 20)]. The $\sigma\sigma$can control the strength of smoothing: the larger σ becomes, the stronger smoothing is and the more noise can be removed. However, the strong smoothing has a risk that textures and edges which have weak intensity signals would be disappeared. Texture-loss would emerge in natural images when we use a large value of σ because the natural images include a lot of weak texture regions in comparison to the artificial images. On the other hand, the artificial images consist of high contrast edges and uniform flat areas; noise can be removed while preserving signals such as strong edges by setting a large σ. Consequently, although we used fixed σ in the previous experiments, σ should be controlled based on the intensities of signal and noise for improving the performance of our EJBF. We are going to optimize the parameters of our EJBF adaptively based on image features as a future work.

Finally, we describe an experimental result regarding computational cost. Table 5 shows the average processing time for 768×512 pixel images. Figure 15 shows a graph of the average ΔPSNR vs. the processing time. The upper left point is more efficient than the lower right one in this graph. In Table 5 and Fig. 15, we can see that the SA-DCT and the BM3D require plenty of time. The processing time of our EJBF was about 1/50 for the SA-DCT and about 1/30 for the BM3D, and ΔPSNR of our EJBF was highest of all comparing methods. Our EJBF achieves high efficiency in terms of the performance and computational cost. Furthermore, we can expect that parallel processing and an implementation method of fast bilateral filter [20)] are useful to improve the processing speed of our EJBF. It would be possible to apply to ultra-high definition video such as 4K and 8K in real-time processing.

5. Conclusion

In this paper, we proposed a simple and effective technique, named extend joint bilateral filter, for achieving improvement of color image quality. Color bleeding, which is annoying chroma artifact due to lossy compression, comes from not only quantization but also sub-sampling in YCbCr 4:2:0 color format. In order to deal with the problems simultaneously, we developed a new filtering method which refers to both of luma and chroma components in an extended framework of the joint bilateral filter. We showed that our method can reduce color artifacts and can improve details while suppressing the side-effect of color edge blurring; experimental results demonstrated that our method improves image quality both objectively and subjectively while saving computational cost.

Acknowledgement

Special thanks to Mr. Ohashi for the helpful advice and constructive discussion. We would also like to express our gratitude to Mr. Yamaguchi, Mr. Takahashi and Ms. Huber for supporting this research work. In addition, we thank all of our team members.

References

1) ITU-T and ISO/IEC, ITU-T Rec. T.81|ISO/IEC 10918-1 (JPEG) (1994)
2) ITU-T and ISO/IEC, ITU-T Rec. T.800|ISO/IEC 15444-1 (JPEG2000) (2000)
3) ITU-T and ISO/IEC, ITU-T Rec. H.262|ISO/IEC 13818-2 (MPEG-2 Video) (1995)
4) ITU-T and ISO/IEC, ITU-T Rec. H.264|ISO/IEC 14496-10 Advanced Video Coding (H.264/AVC) (2003)
5) ITU-T and ISO/IEC, ITU-T Rec. H.265|ISO/IEC 23008-2 High Efficiency Video Coding (H.265/HEVC) (2013)
6) C.J. van den Branden Lambrecht: "Vision Models and Applications to Image and Video Processing", Kluwer Academic Publishers (2001)
7) M. Yuen and H.R. Wu: "A Survey of Hybrid MC/DPCM/DCT Video Coding Distortions", Signal Processing, 70, 3, pp.247-278 (1998)
8) K. Zeng, T Zhao, A. Rehman and Z. Wang: "Characterizing Perceptual Artifacts in Compressed Video Streams", Proc. of SPIE, Human Vision and Electronic Imaging XIX, 9014 (Feb. 2014)
9) C. Tomasi and R. Manduchi: "Bilateral Filtering for Gray and Color Images", IEEE International Conference on Computer Vision, pp.839-846 (Jan. 1998)
10) H. Abbas and L.J. Karam: "Suppression of Mosquito Noise by Recursive Epsilon-filters", IEEE International Conference on Acoustics, Speech and Signal Processing, 1, pp.773-776 (Apr. 2007)
11) H. Takeda: "Kernel Regression for Image Processing and Reconstruction," IEEE Trans. Image Process., 16, 2, pp.349-366 (Feb. 2007)
12) N.C. Francisco, N.M.M. Rodrigues, E.A.B. da Silva and S.M.M. de Faria: "A Generic Post-deblocking Filter for Block Based Image Compression Algorithms", Signal Processing: Image

Communication, Elsevier, 27, 9, pp.985-997 (Oct. 2012)
13) G. Yu and G. Sapiro: "DCT Image Denoising: A Simple and Effective Image Denoising Algorithm", Image Processing On Line (2011): http://dx.doi.org/10.5201/ipol.2011.ys-dct
14) A. Foi, V. Katkovnik and K. Egiazarian: "Pointwise Shape-adaptive DCT for High-quality Denoising and Deblocking of Grayscale and Color Images", IEEE Trans. Image Process., 16, 5, pp.1395-1411 (May 2007)
15) A. Buades, B. Coll and J.M. Morel: "A Non-local Algorithm for Image Denoising", IEEE Computer Vision and Pattern Recognition, 2, pp.60-65 (June 2005)
16) K. Dabov, A. Foi, V. Katkovnik and K. Egiazarian: "BM3D Image Denoising with Shape-adaptive Principal Component Analysis", Proc. Workshop on Signal Processing with Adaptive Sparse Structured Representations (Apr. 2009)
17) T. Komatsu, Y. Ueda and T. Saito: "Super-resolution Decoding of JPEG-compressed Image Data with The Shrinkage in The Redundant DCT Domain", Picture Coding Symposium, pp.114-117 (Dec. 2010)
18) P. Milanfar, "Super-resolution Imaging," CRC Press (2010)
19) D. Glasner, S. Bagon and M. Irani: "Super-resolution from a Single Image", IEEE International Conference on Computer Vision, pp.349-356 (Sep. 2009)
20) S. Paris, P. Kornprobst, J. Tumblin and F. Durand: "Bilateral Filtering: Theory and Applications", Foundations and Trends in Computer Graphics and Vision, 4, 1, pp.1-73 (Aug. 2009)
21) G. Petschnigg, M. Agrawala, H. Hoppe, R. Szeliski, M. Cohen and K. Toyama: "Digital Photography with Flash and No-flash Image Pairs", ACM Transactions on Graphics, 23, 3, pp.664-672 (Aug. 2004)
22) E. Eisemann and F. Durand: "Flash Photography Enhancement via Intrinsic Relighting", ACM Transactions on Graphics, 23, 3, pp.673-678 (Aug. 2004)
23) J. Kopf, M.F. Cohen, D. Lischinski and M. Uyttendaele: "Joint Bilateral Upsampling", ACM Transactions on Graphics, 26, 3, 96 (July 2007)
24) E.P. Bennett, J.L. Mason and L. McMillan: "Multispectral Bilateral Video Fusion", IEEE Trans. Image Process., 16, 5, pp.1185-1194 (May 2007)
25) K. He, J. Sun and X. Tang: "Guided Image Filtering", IEEE Trans. Pattern Analysis and Machine Intelligence, 35, 6, pp.1397-1409 (2013)
26) D. Kiku, Y. Monno, M. Tanaka and M. Okutomi: "Residual Interpolation for Color Image Demosaicking", IEEE International Conference on Image Processing, pp.2304-2308 (Sep. 2013)
27) A. Punchihewa, D.G. Bailey and R.M. Hodgson: "The Development of a Novel Image Quality Metric and a Synthetic Colour Test Image for Objective Quality Assessment of Digital Codecs", TENCON 2005 2005 IEEE Resion 10, p. 1-6 (Nov. 2005)
28) A. Punchihewa and J. Armstrong: "Effects of Sub-sampling and Quantisation on Colour Bleeding due to Image and Video Compression", International Conference on Image and Vision Computing New Zealand, p. 1-6 (No 2008)
29) A. Punchihewa: "Objective Evaluation of Colour Bleeding Artefact due to Image Codecs", International Conference on Visual Information Enginerring, pp.801-806 (July 2008)
30) F. Coudoux, M. Gazalet and P. Corlay: "An Adaptive Postprocessing Technique for the Reduction of Color Bleeding in DCT-coded Images", IEEE Trans. on Circuits and Syst. for Video Tech., 14, 1, pp.114-121 (Jan. 2004)
31) F. Coudoux, M. Gazalet and P. Corlay: "A DCT-domain Postprocessor for Color Bleeding Removal", Proceedings of the 2005 European Conference on Circuit Theory and Design, 1, pp.209-212 (2005)
32) F. Coudoux, M. Gazalet and P. Corlay: "Reduction of Color Bleeding for 4:1:1 Compressed Video", IEEE Trans. Broadcast., 51, 4, pp.538-542 (Dec. 2005)
33) A. Catorina, G. Spampinato, A. Bruna and A. Capra: "Adaptive Color Bleeding Removal for Video and Still DCT Compressed Sequences", Proc. of SPIE, Digital Photography III, 6502 (Feb. 2007)
34) G. Spampinato, A. Castorina, A. Bruna and A. Capra: "JPEG Adaptive Chromatic Post-Processing", International Conference on Image Analysis and Processing Workshops, pp.202-205 (Sep. 2007)
35) S. Li, O.C. Au, L. Sun and W. Dai: "Color Bleeding Reduction in Image and Video Compression", International Conference on Computer Science and Network Technology, 2, pp.665-669 (Dec. 2011)
36) N. Wada, M. Kazui and M. Haseyama: "Extended Joint Bilateral Filtering for Color Noise Reduction and Super Resolution", International Workshop on Advanced Image Technology, pp.212-217 (Jan. 2014)
37) T.Q. Pham and L.J. van Vliet: "Separable Bialteral Filtering for Fast Video Preprocessing", IEEE International Conference on Multimedia and Expo (ICME2005) (July 2005)
38) D. Agarwal, S. Wilf, A. Dhungel and S.K. Prasad: "Acceleration of Bilateral Filtering Algorithm for Manycore and Multicore Architectures", IEEE International Conference on Parallel Processing (ICPP2012) (Sep. 2012)
39) Kodak Lossless True Color Image Suite: http://r0k.us/graphics/kodak
40) Independent JPEG Group JPEG software: http://www.infai.org/jpeg

Naofumi Wada received the B.S. and M.S. degrees in Engineering from Hokkaido University, Japan in 2002 and 2004, respectively. He worked at the Research and Development Center of Toshiba Corporation from 2004 to 2009. He jointed Samsung R&D Institute Japan in 2009. His research interests include image and video processing, video codecs, and computer vision. He is a member of the Institute of Image Information and Television Engineers (ITE).

Masato Kazui received the B.S., M.S., and Ph.D. degrees in Engineering from Hokkaido University, Japan in 1994, 1996, and 2000, respectively. He worked at Hitachi Research Laboratory of Hitachi Ltd. from 2000 to 2009. He was a visiting researcher of Carnegie Mellon University, USA from 2005 to 2006. He joined Samsung R&D Institute Japan in 2009. His research interests include SEM, surveillance systems, digital image processing of digital still camera and TV, and computer vision. He is a member of IEEE, IEICE, and IPSJ.

Miki Haseyama received her B.S., M.S. and Ph.D. degrees in Electronics from Hokkaido University, Japan in 1986, 1988 and 1993, respectively. She joined the Graduate School of Information Science and Technology, Hokkaido University as an associate professor in 1994. She was a visiting associate professor of Washington University, USA from 2005 to 2006. She is currently a professor in the Graduate School of Information Science and Technology, Hokkaido University. Her research interests include image and video processing and its development into semantic analysis. She is a member of the IEEE, IEICE, Institute of Image Information and Television Engineers (ITE) and Acoustical Society of Japan (ASJ).